BLIND ITERATIVE DECONVOLUTION OF ULTRASONIC IMAGES

R. Jiřík* and T. Taxt**

* Dept. of Biomedical Engineering, Brno University of Technology, Brno, Czech Republic
** Dept. of Biomedicine, University of Bergen, Bergen, Norway

jirik@feec.vutbr.cz, Torfinn.Taxt@fys.uib.no

Abstract: A new two-dimensional method for ultrasonic imaging is presented. It increases the spacial resolution of ultrasonic images by postprocessing the raw radiofrequency signal. The approach is based on maximum-likelihood blind deconvolution. The restored true image and the degrading process characteristics are estimated simultaneously based on a-priori constraints.
The approach extends the two-dimensional homomorphic deconvolution concept by using it only for initial estimation. This avoids the limitations of homomorphic deconvolution, namely the need for two-dimensional phase unwrapping and the assumption that the true image and the degradation characteristics are represented by different separate bands in the cepstrum domain.
The algorithm was tested on data acquired from a tissue-mimicking phantom and on clinical data. The observed and measured spacial resolution of the resulting images was substantially increased.

Introduction

The fairly low spatial resolution is one of the major limiting factors in the clinical usefulness of medical ultrasound B-mode images. This is still true, eventhough the spatial image resolution of high end ultrasound scanners has been substantially improved in the last decade.

Ultrasonic images can be modeled as a convolution of the point spread function (PSF) of the imaging process and the tissue function, which characterizes the distribution of specular reflectors and diffuse scatterers in the imaged area. One way to increase the spatial resolution of medical ultrasonic images is by deconvolving the observed radiofrequency image by the PSF.

The PSF is, to large extent, determined by the imaged tissue. Thus, the PSF has to be estimated from the recorded radiofrequency data together with the tissue function, using so called blind deconvolution [1].

There have been several methods to estimate the PSF from the measured radiofrequency data. Most techniques estimate the one-dimensional (1-D) PSF in the axial [2, 3, 4, 5, 6] and in the lateral [6] direction. The 1-D PSF can be estimated from the measured radiofrequency signal using the prediction error algorithm [2], analysis in the real cepstrum [3], complex cepstrum [4] or bicepstrum [6] domain.

In general, the PSF is not separable in the axial and lateral directions. Thus, it has to be estimated as a 2-D function. So far, the only successful 2-D blind deconvolution of ultrasound images has been the approach based on filtering in the 2-D cepstrum domain, also called homomorphic liftering [7, 8, 9, 10]. In this approach, it is assumed that the PSF and the tissue function reside in separate bands of the 2-D cepstrum domain. This simplifying assumption has been the major objection against the approach. Another drawback of the 2-D homomorphic deconvolution is the necessity for 2-D phase unwrapping, which is an ill-posed noise-sensitive problem [11].

In other applications, e.g. astronomy and remote sensing, the blind image deconvolution has been used to much larger extent and these fields can be a good inspiration for deconvolution of ultrasound images. There have been two main approaches to blind image deconvolution [1].

1. Separate estimation of the PSF which is subsequently used in one of the classical deconvolution algorithms. The approach is applicable if the true image includes some special features (e.g. points, edges) or when the PSF is of a special parametric form (e.g. out-of-focus lens system, linear camera motion). A special case falling into this group is homomorphic deconvolution.

2. The second approach is a simultaneous estimation of the PSF and the true image. One class of these methods models the imaging process using autoregressive moving average (ARMA) parameters. The deconvolution problem is formulated as a maximum likelihood estimation [12] or generalized cross-validation [13]. The methods rely on second-order statistics and hence can not retrieve the phase of the PSF. These methods are suitable for applications where the PSF is symmetric or minimum-phase or where strong additional assumptions can be imposed on the PSF. Another approach to simultaneous estimation of the PSF and the true image is nonparametric identification. A classical approach of this class is the iterative blind deconvolution (IBD) [14], known to have poor convergence properties. The drawback is improved by formulating the deconvolution as a nonparametric maximum-likelihood problem [15].

This paper presents a method to improve 2-D homomorphic deconvolution of ultrasound images by means of blind iterative deconvolution. It avoids both the above mentioned limitations of the 2-D homomorphic deconvolution, i.e. the assumption that the PSF and the tissue function lie in different 2-D cepstrum bands and the 2-D

ISSN: 1727-1983

phase unwrapping problem.

2-D homomorphic liftering is used only to obtain an initial estimate of the amplitude response of the degrading system. In the initial estimation, 1-D phase unwrapping is used instead of the 2-D phase unwrapping. Subsequently, blind iterative deconvolution is used to simultaneously estimate the full PSF and the tissue function. Nonparametric blind iterative deconvolution has been chosen and adopted to ultrasound radiofrequency data. The ARMA parameter estimation methods are not suitable in this application because the PSF in ultrasound imaging is not symmetric or minimum-phase in general. The problem is formulated as maximum-likelihood deconvolution and solved using the conjugate gradient optimization method.

Model of Distortion

The input image for the deconvolution is formed by radiofrequency data recorded by a sector scanner. The data are processed in polar coordinates. The distortion of the radiofrequency image can be modeled using a spatially variant linear operator. For a small subimage s of the complete radiofrequency image, spatially invariant distortion can be assumed:

$$g_s(m,n) = f_s(m,n) * h_s(m,n) + w_s(m,n). \qquad (1)$$

The operator $*$ stands for 2-D convolution. m,n are the spatial-domain indices corresponding to the radial and lateral directions. $g(m,n)$ is the received radiofrequency image data. $f(m,n)$ is the tissue function describing the distribution of reflectors and scatterers in the imaged area. $h(m,n)$ is the PSF of the imaging process and $w(m,n)$ is a noise term, accounting for the measurement noise of the electronic circuits.

The PSF in the frequency domain can be modeled as a combination of four components:

$$H_s(\omega_1,\omega_2) = H_{tr}(\omega_1)\cdot S(\omega_1,\omega_2)\cdot P(\omega_1,\omega_2)\cdot A(\omega_1). \qquad (2)$$

$H_{tr}(\omega_1)$ describes the electroacoustical transfer function of the transducer, both on emission and reception, and the electrical excitation of the transducer. It is constant through all subimages of the complete radiofrequency image. $S(\omega_1,\omega_2)$, is a two-dimensional transfer function that relates the transducer geometry to the spatial extent of the ultrasound beam. It describes the diffraction pattern and focusing which determine the beam profile. $S(\omega_1,\omega_2)$ changes with position in the image. $P(\omega_1,\omega_2)$ is the tissue transfer function due to the phase front aberration [16], a phenomenon taking place mainly in the fat layers of the body wall which seriously degrades the spatial resolution. $A(\omega_1)$ accounts for the attenuation of the tissue between the probe and the subimage position and within the subimage itself. It is a 1-D process in the radial direction. Both $P(\omega_1,\omega_2)$ and $A(\omega_1)$ change with position of the subimage because they depend on the tissue.

In the present approach, it is convenient to approximate the spatially variant components $P(\omega_1,\omega_2)$, $A(\omega_1)$ and $S(\omega_1,\omega_2)$ by their global parts. That means that the PSF is assumed spatially invariant in the whole image and the following model of the complete radiofrequency image can be used:

$$g(m,n) = f(m,n) * h(m,n) + w(m,n). \qquad (3)$$

The notation corresponds to the one in Eq. 1. Then, the deconvolution can be applied to the whole image. Thus, only the global degradation is identified and removed from the input radiofrequency data. The locally varying components of $P(\omega_1,\omega_2)$, $A(\omega_1)$ and $S(\omega_1,\omega_2)$ remain present.

Initial Estimation

In blind iterative deconvolution techniques, it is important that the initial estimate of the tissue function and the PSF lie as close to the true values as possible. So far, the most reliable results have been obtained using homomorphic liftering [7, 8, 9]. Hence, the approach was chosen for the initial estimation. The basic idea is to estimate the PSF from the complex-cepstrum-domain representation of the measured radiofrequency image and to use it in Wiener filtering for initial estimation of the tissue function.

The homomorphic transform of the input image (i.e. mapping to the complex cepstrum domain) is divided into homomorphic transform of the amplitude and phase of the input image spectrum.

The amplitude spectrum is obtained from the Fourier transform of a zero-padded image (to avoid cepstrum-domain aliasing [17]). Then the spectrum amplitude is transformed by adding a small constant (to avoid zero values), applying logarithmic transform and finally inverse Fourier transform [7].

In homomorphic mapping of the phase image of the input image spectrum, the 2-D phase unwrapping is avoided by assuming a separable PSF. Then, the task is decomposed to the estimation of the 1-D PSFs in the axial and lateral directions. As shown in [4], the most reliable 1-D method of homomorphic transform is based on polynomial rooting [17]. Thus, the approach was chosen here too. First, all beams of the input image are divided to short overlapping segments. Then the segments are mapped to the complex cepstrum domain and the resulting cepstra averaged. The same procedure is done in the lateral direction. As the PSF in the lateral direction is close to a symmetric signal, i.e. its complex cepstrum is symmetric too [17], symmetry was induced on the lateral-direction cepstrum. In the resulting complex cepstrum of the separable 2-D PSF, the 1-D cepstra of the axial and lateral direction form the corresponding main axes [7].

The complex cepstra of the amplitude and phase of the input image spectrum are combined together to form the complete complex cepstrum of the input image. The complex cepstrum of the initial 2-D PSF is calculated by 2-D Butterworth liftering of the input image data in

ISSN: 1727-1983

the the complex-cepstrum domain [8, 9]. The initial estimate of the PSF is obtained by inverse homomorphic transform.

The initial estimate of the tissue function is obtained by Wiener filtering. It is known that small errors in the PSF give rise to big errors in the Wiener-filtered image. The amplitude spectrum of the initial PSF is estimated more accurately than the phase, which was calculated using the separability assumption and with numerical errors of polynomial rooting. Thus, only the amplitude spectrum information of the PSF is used for the Wiener filter, while the phase is set to zero (meaning 2-D symmetry of the PSF in the spatial domain). The signal-to-noise ratio used in the Wiener filter is assumed constant.

Blind Iterative Deconvolution

The blind iterative deconvolution is formulated as maximum likelihood estimation of the PSF and the tissue function. It is derived from the statistics of the noise term $w(m,n)$. For ultrasound images, a Gaussian noise model is often used. This leads to the following form of the maximum likelihood term [15]

$$\varepsilon_{ML} = \sum_{m,n} |g(m,n) - h(m,n) * f(m,n)|^2. \qquad (4)$$

The pixels of the PSF and the tissue function are estimated by minimizing ε_{ML}. Conjugate gradient optimization is used here. The first derivative of the criterial function, required by the algorithm, is derived analytically [15].

The iterative deconvolution algorithms are known to converge to local extrema of the criterial function. To obtain an estimate which is closer to the true values, it is necessary to introduce additional constraints. A known support region is supposed for the tissue function and the PSF. All values outside the support region are assumed zero. The support region of the tissue function is identical to the size of the input radiofrequency image. The PSF support region is set to the assumed size of the PSF, based on PSF measurements. To keep the energy of the updated PSF on a constant level, it is forced to have unity energy. Furthermore, zero mean value is induced to the PSF.

The support-region constraint is directly incorporated in the optimization algorithm. The unity-energy constraint is applied as a strict constraint, similarly to [15]. Here, it is formulated as the following substitution:

$$h(m,n) = \frac{\psi(m,n)}{\sqrt{\sum_{m,n} \psi(m,n)}}. \qquad (5)$$

A similar substitution follows for the zero-mean constraint:

$$\psi(m,n) = \phi(m,n) - \frac{1}{MN} \sum_{m,n} \phi(m,n), \qquad (6)$$

where M and N are the extents of the PSF in the axial and lateral directions.

Then, the optimized variables are the values (pixels) $f(m,n)$ and $\phi(m,n)$. The derivative of the criterial function is modified to account for both substitutions.

Experimental data and parameter values

The deconvolution method was tested on image sequences recorded from a tissue-mimicking phantom Gammex 403GS and on clinical images of kidney, aorta and heart. All image sequences were recorded using GE Vingmed Ultrasound System 5 scanner, with a phased array probe FPA 64 2.5c (64 elements, nominal frequency 2.5 MHz). Raw radiofrequency image data after quadrature demodulation were used (demodulation frequency 2.2 MHz, sampling frequency after demodulation 3.3 MHz).

The phantom data were recorded from an imaged region covering 5 point targets. The phantom sequence consisted of 6 frames. The clinical image sequences consisted each of 10 images.

The Butterworth filter used in the cepstrum-domain low-pass liftering was of order 5 and the radial and lateral locus values were 3 and 2, respectively. The approximate values were determined from the log-spectrum of the recorded radiofrequency signals as described in [18] and then further experimentally adjusted to give the best results.

The number of iterations used in the conjugate gradient optimization was 45. With further iterations, the improvement of the spatial resolution became negligible, with increasing noise level. The noise-to-signal constant of the Wiener filter was 0.05 as the value giving the highest spatial resolution without decreasing the signal-to-noise ratio in the image.

Evaluation procedure

An exact evaluation of the deconvolution performance is possible if the true image is known. This was the case of data recorded from the used phantom. The resolution was evaluated, from the polar-coordinate representation envelope images of nylon wires located perpendicularly to the tomographic plane of the image. An image of such point targets gives an estimate of the 2-D point spread function at the current position (distorted by surrounding diffuse scatterers). For each point target, a small image area was selected covering the complete point spread function. Then, the corresponding envelope subimage was normalized and the size of the point spread function was measured as the area under the pixels with values higher than 0.5

For clinical recordings, the true images are not known, thus, there is no exact quantitative method to evaluate the resolution improvement of the deconvolved images. However, as shown in previous papers on deconvolution of ultrasonic images [6, 7, 4, 5, 9], the resolution gain can be estimated visually or quantitatively using an autocorrelation criterion.

ISSN: 1727-1983

The visual evaluation is possible for image areas showing structures with well defined borders, e.g. myocard and vessels. The sharpness and continuity of the borders is a good measure of the spatial resolution. Furthermore, higher spatial resolution is also indicated by finer speckle pattern, as the spatial correlation of speckles increases with the extent of the point spread function.

The autocorrelation measure was used as follows. First, the 2-D autocorrelation was computed from the envelope of the polar coordinate representation of the input and deconvolved images. The number of pixels of the normalized autocorrelation function with value higher than 0.75 (corresponding to a 2.5 dB reduction) was counted in the original and the deconvolved images. The ratio between these numbers was taken as the numeric measure of the resolution gain.

To evaluate the effect of deconvolution on the noise level, the spatial signal-to-noise ratio was estimated. In image processing applications, the noise power S_{ww} is estimated as the average of squared pixel values within a region containing only noise. The average of squared pixel values within the complete image, S_{gg} estimates the sum of the noise power S_{ww} and the signal power S_{ff}. The signal-to-noise ratio is then estimated as $\frac{S_{gg}-S_{ww}}{S_{ww}}$.

For ultrasonic images, the homogeneous regions would correspond to regions with no reflectors and scatterers. Such regions do not exist in real tissues. Image regions of low echogeneity (blood areas, kidney cortex) were chosen here as the closest approximation of such regions. The computations were done on the radiofrequency data representation.

Results

The spatial quality was assessed for the input image, initial homomorphic deconvolution estimate and for the output of the iterative deconvolution. The results (Table 1) show that the spatial resolution was increased in the initial estimate and further improved by the iterative deconvolution. The signal-to-noise ratio remained unchanged (Table 1).

Table 1: Size of the PSF measured on phantom data (mean $\pm$ std.dev.) and signal-to-noise ratios (SNR)

Image sequence	PSF size [mm x rad]	SNR [dB]
Input image	0.052 ± 0.016	21.8 ± 0.02
Initial estimate	0.045 ± 0.023	22.6 ± 0.10
Iterative deconv.	0.039 ± 0.021	22.8 ± 0.10

Same effects of the iterative deconvolution were observed on clinical images. The spatial resolution was significantly increased in the initial estimate. Further improvement by iterative deconvolution was observed, but the increase in the spatial resolution was smaller. This was observed visually as increased sharpness of the kidney capsule, delineation of aorta and liver vessels and better definition of myocard. Also the speckle pattern of the deconvolved images was more distinct with much shorter spatial correlation. An example is shown in Fig. 1. The autocorrelation measure of the spatial resolution gain confirms the visual observation (Table 2).

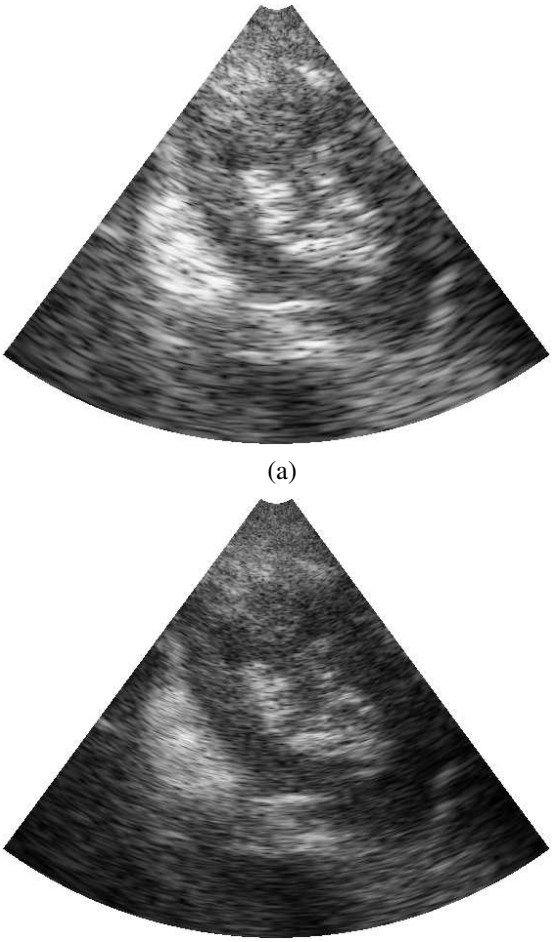

(a)

(b)

Figure 1: Images of kidney. (a) Original image. (b) Iterative deconvolution result.

Table 2: Resolution gain of the deconvolved images (mean $\pm$ std.dev.)

Image sequence	Resolution gain (initial est.)	Resolution gain (iterative deconv.)
kidney	2.9 ± 0.3	3.3 ± 0.2
heart	3.3 ± 0.2	3.7 ± 0.2
aorta/liver	2.8 ± 0.1	3.0 ± 0.1

The estimates of the spatial signal-to-noise ratio (Table 3) indicate that neither homomorphic deconvolution nor the subsequent iterative deconvolution affect negatively the noise level of images.

ISSN: 1727-1983

Table 3: Spatial signal-to-noise ratios of the input images, initial estimates and images after iterative deconvolution

Image sequence	SNR [dB] input	(initial est.)	(iter. dec.)
kidney	8 ± 2	9 ± 1	9 ± 1
heart	8 ± 3	7 ± 3	7 ± 3
aorta/liver	18 ± 2	17 ± 1	17 ± 2

Discussion and conclusion

A new 2-D deconvolution technique for ultrasound imaging has been presented. The approach is based on maximum-likelihood blind deconvolution. The tissue function and the PSF are estimated simultaneously based on a-priori constraints.

The approach extends the two-dimensional homomorphic deconvolution concept by using it only for initial estimation. This avoids the limitations of homomorphic deconvolution, namely the need for 2-D phase unwrapping and the assumption that the tissue function and the PSF are represented by different separate bands in the cepstrum domain.

The presented method is focused only on estimation and removal of the global part of the PSF. This enabled the deconvolution of the whole radiofrequency image, which made it more reliable and faster than the deconvolution of small subimages [9] which would, on the other hand, take also the spatially variant PSF components into account.

Both parts of the algorithm, i.e. the homomorphic and iterative deconvolutions, can be further improved. The initial estimate could be improved by applying some new noise-robust 2-D phase unwrapping methods (e.g. [10]). The Blind iterative deconvolution step is expected to give better results by applying more a priori constraints on the estimated functions in combination with more advanced deconvolution methods.

Acknowledgments

The project has been supported by the Czech Ministry of Education, Youth and Sports (grants no. 1K03017, MS0021630513). We are also grateful to GE Vingmed Ultrasound a.s. for making the recording of raw radiofrequency signals possible and to Trygve Hausken and Johan Kirkhorn for their consultations concerning image recording and data format of the used ultrasound scanner.

References

[1] KUNDUR, D. D. HATZINAKOS: *Blind Image Deconvolution*. IEEE Signal Processing Magazine, 13(3):43–64, 1996.

[2] JENSEN, J. A.: *Deconvolution of Ultrasound Images*. Ultrasonic Imaging, 14(1):1–15, 1992.

[3] JENSEN, J. A. S. LEEMAN: *Nonparametric Estimation of Ultrasound Pulses*. IEEE Trans. Biomed. Eng., 41(10):929–936, 1994.

[4] TAXT, T.: *Comparison of Cepstrum Based Methods for Radial Blind Deconvolution of Ultrasound Images*. IEEE Trans. Ultrason. Ferroelec. Freq. Cont., 44(3):666–674, 1997.

[5] ADAM, D. O. MICHAILOVICH: *Blind Deconvolution of Ultrasound Sequences Using Nonparametric Local Polynomial Estimates of the Pulse*. IEEE Trans. Biomed. Eng., 49(2):118–131, 2002.

[6] ABEYRATNE, U. R., A. P. PETROPULU, J. M. REID, T. GOLAS, E. CONANT F. FORSBERG: *Higher order versus second order statistics in ultrasoundn image deconvolution*. IEEE Trans. Ultrason. Ferroelec. Freq. Cont., 44(6), 1997.

[7] TAXT, T.: *Restoration of Medical Ultrasound Images Using Two-Dimensional Homomorphic Deconvolution*. IEEE Trans. Ultrason. Ferroelec. Freq. Cont., 42:543–554, 1995.

[8] TAXT, T. J. STRAND: *Two-Dimensional Noise-Robust Blind Deconvolution of Ultrasound Images*. IEEE Trans. Ultrason. Ferroelec. Freq. Cont., 48(4):861–866, 2001.

[9] TAXT, T. R. JIŘÍK: *Superresolution of Ultrasound Images Using the 1st and 2nd Harmonic Signal*. IEEE Trans. Ultrason. Ferroelec. Freq. Cont., 51(2):163–175, 2004.

[10] MICHAILOVICH, O. D. ADAM: *Phase unwrapping for 2-D blind deconvolution of ultrasound images*. IEEE Trans. Med. Imag., 23(1):7–25, 2004.

[11] GHIGLIA, D. C. M. D. PRITT: *Two-Dimensional Phase Unwrapping: Theory, Algorithms and Software*. John Wiley & Sons, Inc., 1998.

[12] LAGENDIJK, R. L., A. M. TEKALP J. BIEMOND: *Maximum Likelihood Image and Blur Identification: a Unifying Approach*. Optical Engineering, 29(5):422–435, 1990.

[13] REEVES, S. J. R. M. MERSEREAU: *Blur Identification by the Method of Generalized Cross-Validation*. IEEE Trans. Image Processing, 1(3):301–311, 1992.

[14] AYERS, G. R. J. C. DAINTY: *Iterataive Blind Deconvolution Method and Its Applications*. Opt. Lett., 13(7):547–549, 1988.

[15] THIBAUT, E. J.-M. CONAN: *Strict A Priori Constraints for Maximum-Likelihood Blind Deconvolution*. J. Opt. Soc. Am. A, 12(3):458–491, 1995.

[16] ANGELSEN, B.: *Ultrasound Imaging: Waves, Signals, and Signal Processing*. Emantec, Trondheim, Norway, 2000.

[17] OPPENHEIM, A. V. R. W. SCHAFER: *Discrete Time Signal Processing*. Prentice Hall, 1989.

[18] JENSEN, J. A.: *Estimation of In Vivo Pulses in Medical Ultrasound*. Ultrasonic Imaging, 16(3):190–203, 1994.

ISSN: 1727-1983